Communication

Nitrosyl Linkage Isomers: NO Coupling to NO at a Mononuclear Site

Subrata Kundu, Phan N. Phu, Pokhraj Ghosh, Stosh A. Kozimor, Jeffery A. Bertke, S. Chantal E. Stieber, and Timothy H. Warren

J. Am. Chem. Soc., **Just Accepted Manuscript** • DOI: 10.1021/jacs.8b09769 • Publication Date (Web): 02 Jan 2019

Nitrosyl Linkage Isomers: NO Coupling to N_2O at a Mononuclear Site

Subrata Kundu,[a,b] Phan N. Phu,[c] Pokhraj Ghosh,[a] Stosh A. Kozimor,[d] Jeffery A. Bertke,[a] S. Chantal E. Stieber,*[,c,d] and Timothy H. Warren*[,a]

[a]Department of Chemistry, Georgetown University, Box 571227-1227, Washington, D. C. 20057 United States

[b]School of Chemistry, Indian Institute of Science Education and Research Thiruvananthapuram, Kerala 695551, India

[c]California State Polytechnic University, Pomona, California 91768, United States

[d]Los Alamos National Laboratory, MS K558, Los Alamos, New Mexico 87545, United States

Supporting Information Placeholder

ABSTRACT: Linkage isomers of reduced metal-nitrosyl complexes serve as key species in nitric oxide (NO) reduction at monometallic sites to produce nitrous oxide (N_2O), a potent greenhouse gas. While factors leading to extremely rare side-on nitrosyls are unclear, we describe a pair of nickel-nitrosyl linkage isomers through controlled tuning of non-covalent interactions between the nitrosyl ligands and differently encapsulated potassium cations. Furthermore, these reduced metal-nitrosyl species with N-centered spin density undergo radical coupling with free NO and provide a N-N coupled *cis*-hyponitrite intermediate whose protonation triggers the release of N_2O. This report outlines a stepwise molecular mechanism of NO reduction to form N_2O at a mononuclear metal site that provides insight into the related biological reduction of NO to N_2O.

Nitrous oxide (N_2O) is a long-lived (*ca.* 114 years) greenhouse gas with a global warming potential 298 times that of CO_2 on a molecular basis.[1] Enhanced through feeding of crops with nitrogen-rich fertilizers,[2] global emission of N_2O is mainly attributed to the microbial and fungal denitrification processes mediated by metalloenzymes.[3] The most critical step for N_2O formation is N-N bond formation that occurs via the reductive coupling of two nitric oxide (NO) molecules. This takes place at diiron sites of nitric oxide reductase (NOR) enzymes[4] as well as at mononuclear sites in the iron-based cytochrome P450 nitric oxide reductase (NOR)[5] or copper nitrite reductase (CuNiR)[6] enzymes (Figure 1a). Based on numerous theoretical studies, it seems likely that an intermediate hyponitrite species ($N_2O_2^{2-}$) precedes N_2O release.[7] For instance, coupling of two metal-nitrosyl [M]-NO moieties takes place upon reduction of $[(TpRuNO)_2(\mu\text{-Cl})(\mu\text{-Pz})]^{2+}$ to afford the N-N reductively coupled product $(TpRu)_2(\mu\text{-Cl})(\mu\text{-Pz})\{\mu\text{-}\kappa^2\text{-N(=O)N(=O)}\}$.[8] Reductive coupling of NO at copper(I) complexes has led to dinuclear *trans*-hyponitrite copper(II) complexes $[Cu^{II}]_2(O_2N_2)$ that release N_2O either upon acidification[9] or thermal decay;[10] the later also produces $[Cu^{II}](NO_2)$ via disproportionation.[10] The nickel nitrosyl $[(bipy)(Me_2phen)NiNO][PF_6]$ mediates NO disproportionation in the presence of NO and yields N_2O via a mononuclear *cis*-hyponitrite $[Ni](\kappa^2\text{-}O_2N_2)$.[11] The factors that lead to N-N bond formation at a monometallic site, however, have not been explicitly documented.[12]

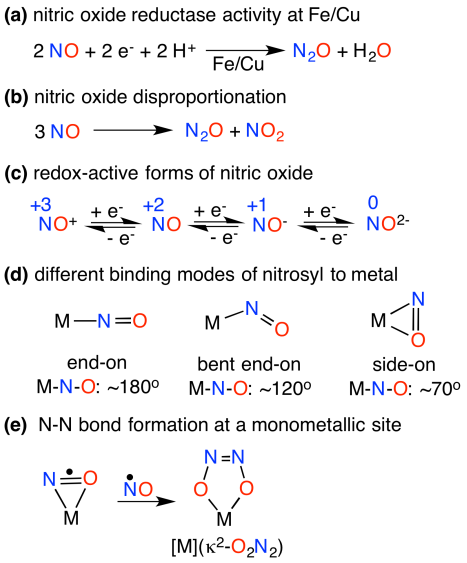

Figure 1. Reactivity and binding of nitrosyl ligands at transition metal sites.

We hypothesize that the presence of spin density at the N atom of a metal-nitrosyl [M]-NO, perhaps enhanced by the ability to achieve a side-on [M]-NO conformation, may facilitate N-N bond formation between a metal-nitrosyl and nitric oxide to give *cis*-hyponitrites $[M](\kappa^2\text{-}O_2N_2)$ (Figure 1e). Access to side-on $[M](\eta^2\text{-NO})$ complexes may both expose the N atom for N-N coupling and initiate a M-O interaction prior to forming mononuclear $[M](\kappa^2\text{-}O_2N_2)$ complexes. Such side-on conformations are known in the photoexcited states of $\{Ni(NO)\}^{10}$ complexes[13] where the superscript in the Enemark-Feltham formulation $\{Ni(NO)\}^{10}$ represents the total number of metal d and NO π* electrons.[14] The side-on binding of a nitrosyl ligand (Figure 1c) in a mononuclear synthetic complex, however, has not been observed in its ground state. $\{[(Me_3Si)_2N]_2(THF)Y\}_2(\mu\text{-}\eta^2\text{:}\eta^2\text{-NO})$ is a singular example that possesses a side-on NO achieved via bridging between two transition or rare earth metal centers that possesses a highly reduced NO^{2-} ligand.[15] Crystallographic studies revealed side-on η^2-NO binding in fully reduced bovine cytochrome c oxidase (CcO)[16] and copper nitrite reductase (CuNiR)[17] that feature mononuclear $\{Cu(NO)\}^{11}$ sites, though solution spectroscopic studies suggest end-on binding.[18,19] DFT calculations for both side-on and end-on $\{Cu(NO)\}^{11}$ species suggest that each possesses a $Cu^{I}(\bullet NO)$ electronic formulation[20] with a considerable

amount of spin density at the nitrosyl N atom, reinforced by EPR studies of the reduced $\{Cu(NO)\}^{11}$ intermediate of CuNIR.[18,21] Furthermore, differential H-bonding and/or steric interactions from second-sphere protein residues may play a vital role in the determining the conformation of $\{Cu(NO)\}^{11}$ species.[21,22]

To synthetically outline factors that control metal-nitrosyl bonding modes and NO coupling reactivity, we targeted low coordinate $\{M(NO)\}^{10/11}$ pairs that could accommodate both side-on NO and *cis*-hyponitrite ligands (Figures 1d and 1e). The salt metathesis reaction between equimolar amounts of the *β*-diketiminato potassium salt $[^{i}Pr_2NN_{F6}]K(THF)$ and $(THF)_2Ni(NO)I$ in tetrahydrofuran (THF) affords the diamagnetic $\{Ni(NO)\}^{10}$ complex $[^{i}Pr_2NN_{F6}]NiNO$ (**1**) isolated as dark green crystals in 76% yield (Figure 2a). The X-ray structure of **1** reveals a trigonal-planar Ni center with an end-on nitrosyl ligand (Ni1-N3-O1 = 174.47(11)°) with a N3-O1 distance of 1.1602(15) Å (Figure S22). The infrared spectrum of **1** indicates a nitrosyl stretch (ν_{NO}) at 1825 cm^{-1}, similar to values reported for other three-coordinate neutral nickel-nitrosyl complexes (ν_{NO} =1817-1779 cm^{-1}).[23] Notably, the cyclic voltammogram of **1** in tetrahydrofuran at room temperature exhibits a reversible reduction wave centered at -1.89 V (*vs* ferrocenium/ferrocene), attributed to the $\{Ni(NO)\}^{10}/^{11}$ redox couple (Figure S6).

One-electron reduction of the $\{Ni(NO)\}^{10}$ complex **1** with potassium-graphite (KC_8) (1.2 equiv) in tetrahydrofuran in the presence of 18-crown-6 (1 equiv) leads to a rapid color change from green to purple (Figure 2a). Single crystal X-ray diffraction analysis of the purple complex **2a** reveals two independent $[^{i}Pr_2NN_{F6}]Ni(\mu\text{-}\eta^2\text{:}\eta^2\text{-NO})K(18\text{-crown-6})(THF)$ moieties. Each nickel exhibits square planar coordination that features a side-on NO ligand between the Ni and K centers. Although disorder from interchange of N/O positions precludes a detailed assessment of metrical parameters, refinement of the NO ligand into a single orientation (Figure 2b) gives short Ni-N (1.853(5) Å; 1.866(5) Å) and Ni-O (1.839(5) Å; 1.868(5) Å) distances similar to those observed in a related $[Ni](\eta^2\text{-ONPh})$ complex.[24] The nitrosyl ligand in the $\{Ni(NO)\}^{11}$ species **2a** (molecule 1: 1.270(6) Å; molecule 2: 1.284(6) Å) is significantly more activated than in the $\{Ni(NO)\}^{10}$ analogue **1** (1.1602(15) Å), despite N/O positional disorder that likely underestimates the N-O distance.[15] Disorder models that allow pairs of N/O atoms to refine lead to slightly longer N-O distances of 1.28 - 1.32 Å but with a wider spread of Ni-N/O distances (Figures S23c and S23d). Thus, **2a** possesses a nitrosyl ligand with a N-O distance longer than in most metal-nitrosyls[25] except $\{[(Me_3Si)_2N]_2(THF)Y\}_2(\mu\text{-}\eta^2\text{:}\eta^2\text{-NO})$ which also features a side-on NO ligand (N-O: 1.390(4)Å).[15] Coordination of the potassium cation to both the nitrogen and oxygen atoms of the reduced nitrosyl ligand in the $\{[Ni](\eta^2\text{-NO})\}^{-}$ anion of **2a** gives K-N/O distances in the range 2.826(5) Å - 2.869(5) Å that leads to Ni···K separations of 4.417 Å (molecule 1) and 4.467 Å (molecule 2). The infrared spectra of two isotopologues **2a** and **2a**-^{15}N exhibit $^{14}N/^{15}N$ isotope sensitive bands at 894 cm^{-1} and 878 cm^{-1}, respectively. This is the lowest ν_{NO} reported for a transition metal nitrosyl complex, lower than 951 cm^{-1} in $\{[(Me_3Si)_2N]_2(THF)Y\}_2(\mu\text{-}\eta^2\text{:}\eta^2\text{-NO})$.[15]

More completely encapsusulating the K+ cation changes the nitrosyl bonding mode of the $\{[Ni](NO)\}^{-}$ anion. Reduction of $[^{i}Pr_2NN_{F6}]NiNO$ (**1**) with KC_8 (1.2 equiv) in the presence of [2.2.2]-cryptand (1 equiv) in tetrahydrofuran gives $[^{i}Pr_2NN_{F6}]Ni(\mu\text{-NO})K[2.2.2\text{-cryptand}]$ (**2b**) (Figures 2c, S24). By significantly lengthening the Ni···K separation (5.466 Å), the nitrosyl ligand exhibits both linear (77%) and side-on (23%) conformations in the solid state. The linear NO ligand (Ni1-N3A-O1A, 165.8(3)°) is more highly reduced than of **1** with a N-O distance of 1.198(4) Å. The minor side-on conformer exhibits N/O positional disorder whose principle component possesses a N-O distance of 1.274(19) Å similar to **2a**. The IR spectrum of a solid sample of **2b** reveals an NO stretch at 1555 cm^{-1} (1525 cm^{-1} for **2b**-^{15}NO) that is consistent with a highly reduced linear NO ligand (Figure S10).[25]

The room temperature EPR spectrum of $[^{i}Pr_2NN_{F6}]Ni(\mu\text{-}\eta^2\text{:}\eta^2\text{-NO})K[18\text{-crown-6}](THF)$ (**2a**) in tetrahydrofuran indicates a S = ½ species with a g_{iso} value of 2.0008 very close to that of the free electron (g_e = 2.0023). This three line spectrum of **2a** is due to strong coupling with the ^{14}N nucleus of the bound NO ligand (A_{14N} = 28.9 MHz) which shifts to a two line pattern for **2a**-^{15}N (A_{15N} = 40.1 MHz) (Figures 3a and 3b). These data are very similar to the highly reduced, radical NO^{2-} dianion in $\{[(Me_3Si)_2N]_2(THF)Y\}_2(\mu\text{-}\eta^2\text{:}\eta^2\text{-NO})$.[15] In both THF solution and frozen glass (20 K), EPR spectra of **2a** and **2b** are nearly indistinguishable (Figures S20 and S21). Modeling of the low T EPR spectra of **2a** was guided by DFT calculations and required the use of two separate components, suggesting that THF solutions of **2a** and **2b** may contain a mixture of side-on and linear nitrosyls.

Ni K-edge X-ray absorption spectroscopy (XAS) probes the Ni oxidation state by exciting a Ni 1s electron to valence Ni 3d orbitals (pre-edge, ~8330-8335 eV) and Ni 4p orbitals (edge,

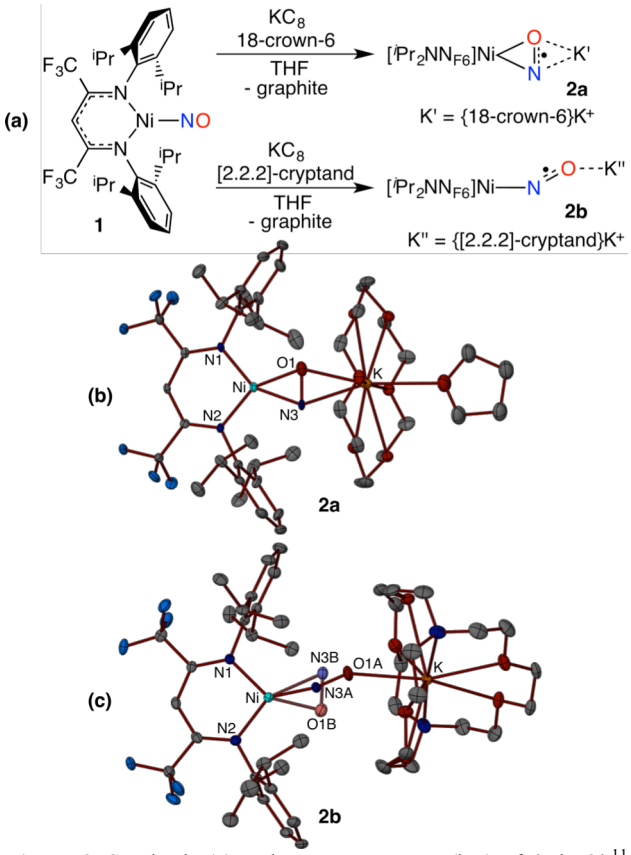

Figure 2. Synthesis (a) and X-ray structures (b,c) of $\{NiNO\}^{11}$ anions **2a** (side-on) and **2b** (77 / 23 end-on / side-on).

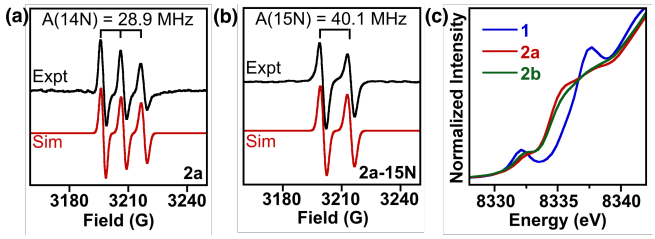

Figure 3. (a, b) X-band EPR spectra (black trace) of **2a** and **2a**-^{15}N in tetrahydrofuran at 293 K. Simulations (red trace) provide g_{iso} = 2.0008, $A_{iso}(^{14}N)$ = 28.9 MHz (for **2a**), and $A_{iso}(^{15}N)$ = 40.1 MHz (for **2a**-^{15}N). (c) Ni K-edge X-ray absorption spectra of **1**, **2a**, and **2b**.

>8345 eV) (Figure 3c). The pre-edge features of **1** (8332.1(0) eV), **2a** (8332.3(1) eV), and **2b** (8332.3(0) eV) are at a similar energy to the closely related Ni^{II} complex $[^{t}Pr_2NN_{F6}]Ni^{II}(\mu\text{-}Br)_2Li(THF)_2$, (8331.6 eV),[24] suggesting that complexes **1**, **2a**, and **2b** are best described as Ni^{II}, with the slight shift to higher pre-edge energies attributed to NO backbonding. Calculated TDDFT XAS assign the rising edge feature in **2a** and **2b** at ~ 8335 eV is a Ni to ligand π* transition that has much weaker intensity in **1** (Figure S38). These results suggest that reduction of $\{Ni(NO)\}^{10}$ species **1** to anionic $\{Ni(NO)\}^{11}$ species **2a** and **2b** occurs primarily at the NO ligand. Complexes **2a** (side-on) and **2b** (principally end-on) have nearly identical XAS spectra and cannot be readily distinguished by this technique.

DFT calculations (Supporting Information) provide insight into electronic structure of the NO complexes and the secondary sphere interactions that control the NO bonding mode. DFT geometry optimizations of **1** and **2a** and **2b** without counterions using the ORCA program[26] (B3LYP, TZVP/SV(P)) reveal spin density at the NO ligand in the **2a** side-on (1.25 e^-) and **2b** end-on conformations (1.52 e^-) that are almost identical in energy. Similar to TpNiNO with a linear NO ligand,[27] complex **1** is best described as high spin Ni(II) antiferromagnetically coupled to NO^{1-} while the anionic complexes **2a** and **2b** are low spin Ni(II) with an NO^{2-} ligand (Figures S33 and S35). Full molecule calculations could energetically distinguish the end-on and side on conformations by fixing the Ni-K distance to 5.466 Å. This revealed the side-on conformation to be only 2.3 kcal/mol more stable, consistent with the linear / side-on disordered observed in the solid state structure of **2b**.

The reduced NO ligands that bear significant unpaired electron density in **2a** and **2b** are primed for coupling with •NO to form *cis*-hyponitrite ligands in complexes $\{[Ni](\kappa^2\text{-}O_2N_2)\}^-$ (**3a** and **3b**). Addition of 1 equiv $NO_{(g)}$ to **2a** in tetrahydrofuran at room temperature affords diamagnetic $\{[^{t}Pr_2NN_{F6}]Ni(\kappa^2\text{-}O_2N_2)\}K(18\text{-crown-6})$ (**3a**) in 72% yield (Figure 4a). X-ray diffraction analysis of **3a** reveals a square planar Ni center with short Ni-$N_{\textit{β}\text{-dik}}$ 1.8895(15), 1.8936(15) Å and Ni-O 1.8241(13), 1.8187(13) Å) distances clearly indicating coupling between the two NO ligands (N3-N4 = 1.235(2) Å) (Figures 4b, S24). The *cis*-hyponitrite ligand exhibits an otherwise symmetric structure (O1-N3 = 1.370(2), O2-N4 = 1.367(2) Å) similar to those previously observed[12] despite unsymmetrical coordination of $\{K[18\text{-crown-}6]\}^+$ cation to both the N atoms of the hyponitrite ligand (K1-N4, 2.7519(17), K1-N3, 3.0584(18) Å). Addition of NO to **2b** similarly provides $\{[^{t}Pr_2NN_{F6}]Ni(\kappa^2\text{-}O_2N_2)\}K[2.2.2\text{-cryptand}]$ (**3b**) in 89% yield with very similar metrical parameters for the

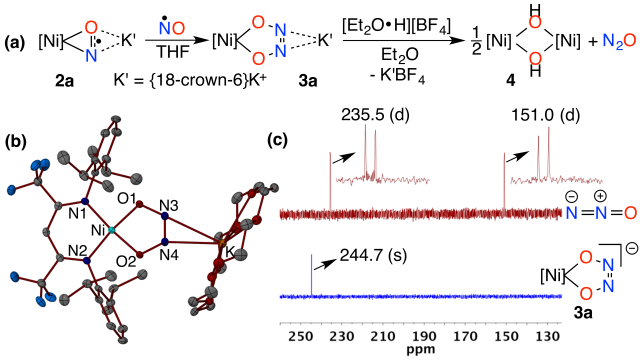

Figure 4. (a) Formation of *cis*-hyponitrite intermediate **3a** and its transformation to nitrous oxide. (b) X-ray crystal structure of 3a. (c) Comparison of ^{15}N NMR spectra (41 MHz, 298 K, tetrahydrofuran-d_8) of $[Ni](\kappa^2\text{-}O_2{}^{15}N_2)K[18\text{-crown-6}]$ (**3a**-$^{15}N^{15}N$) (blue trace) and the crude reaction mixture (red trace) obtained upon addition of 1 equiv trifluoroacetic acid to a solution of **3a**-$^{15}N^{15}N$ in tetrahydrofuran-d_8.

$\{[Ni](\kappa^2\text{-}O_2N_2)\}^-$ moiety that is coordinated to only one *cis*-hyponitrite N atom by the $\{K[2.2.2\text{-cryptand}]\}^+$ cation (K-N = 3.274 Å) (Figure S26). Capture of NO by a reduced NO ligand in $\{[Ni](NO)\}^-$ to form *cis*-hyponitrites $\{[Ni](\kappa^2\text{-}O_2N_2)\}^-$ mirrors the reactivity of NO with $[^{t}Pr_2NN_{F6}]Ni(\eta^2\text{-ONPh})$ to form $[^{t}Pr_2NN_{F6}]Ni(\eta^2\text{-}O_2N_2Ph)$. In both anionic $\{[Ni](NO)\}^-$ and neutral $[Ni](\eta^2\text{-ONPh})$, there is significant unpaired electron density at the reduced NO moiety.[24] Notably, the $\{Ni(NO)\}^{10}$ complex **1** does not react with nitric oxide.

NMR spectra of $\{[^{t}Pr_2NN_{F6}]Ni(\kappa^2\text{-}O_2N_2)\}K[18\text{-crown-6}]$ (**3a**) in THF-d_8 exhibits sharp resonances characteristic of diamagnetic *β*-diketiminato Ni^{II} complexes (Figures S12-S14).[24] Notably, the ^{15}N NMR spectrum of a ^{15}N enriched sample of **3a** (**3a**-$^{15}N^{15}N$) in THF-d_8 shows a sharp singlet at 244.7 ppm (*vs.* liquid NH_3) indicating symmetric κ^2-*O,O* binding of the hyponitrite ligand to the $[^{t}Pr_2NN_{F6}]Ni$ core in solution at room temperature. The $\{[^{t}Pr_2NN_{F6}]Ni(\kappa^2\text{-}O_2N_2)\}^-$ anion in **3b** exhibits identical NMR features as found in **3a**.

Hyponitrite complexes are known to release N_2O upon heating or protonation.[9,10,12] The $\{[^{t}Pr_2NN_{F6}]Ni(\kappa^2\text{-}O_2N_2)\}^-$ anion (in **3a** or **3b**) is thermally stable up to 60 °C with no evidence of N_2O loss. Protonation of **3a** or **3b** by 1 equiv. trifluoroacetic acid, however, triggers the instantaneous release of N_2O observed by ^{15}N NMR (Figures 4c and S17) and IR spectroscopy (2227 cm^{-1}) (Figure S16). Protonation with HBF_4•OEt_2 produces N_2O in 76% yield and allows for isolation of the nickel(II) hydroxide dimer $\{[^{t}Pr_2NN_{F6}]Ni\}_2(\mu\text{-}OH)_2$ (**4**) in 66% yield that exhibits a structure similar to other *β*-diketiminato $[Ni^{II}]_2(\mu\text{-}OH)_2$ complexes (Figure S27).[28]

Spectroscopic and computational insights reveal that one-electron reduction of the $\{Ni(NO)\}^{10}$ complex **1** largely takes place at the NO ligand, leading to side-on and end-on $\{Ni(NO)\}^{11}$ species **2a** and **2b**, respectively. Regardless of the nitrosyl binding mode, these $\{Ni(NO)\}^{11}$ complexes possess a significant amount of unpaired electron density at the nitrosyl N atom and undergo facile coupling with NO to give the *cis*-hyponitrite $\{[Ni](\kappa^2\text{-}O_2N_2)\}^-$ which releases N_2O upon protonation. Controlled tuning of the second coordination sphere interactions between the nitrosyl ligand of the $\{Ni(NO)\}^{11}$ anion and a potassium cation modifies the metal-nitrosyl bonding mode, favoring side-on $[M](\eta^2\text{-NO})$ at shorter Ni···K distances. Especially since the corresponding $\{Ni(NO)\}^{10}$ species does not react with NO, these findings underscore electronic and conformational factors that favor NO coupling via N-N bond formation at monometallic sites. Separation of NO-based reduction and NO coupling steps provides important context for the biologically important reduction of NO that results in N_2O formation via protonation of *cis*-hyponitrite intermediates.

ASSOCIATED CONTENT

Supporting Information. This material is available free of charge via the Internet at http://pubs.acs.org.

Experimental, characterization, and computational details (PDF)

X-ray crystallographic data of **1**, **2a**, **2b**, **3a**, **3b**, and **4** (CIF).

AUTHOR INFORMATION

Corresponding Authors

thw@georgetown.edu (T.H.W.); sestieber@cpp.edu (S.C.E.S)

ACKNOWLEDGMENT

T.H.W. acknowledges the NSF (CHE-1459090), the NIH (R01GM126205), and the Georgetown Environment Initiative. S.C.E.S. acknowledges the CPP College of Science, a CSUPERB

New Investigator Grant, and NSF XSEDE (CHE160059). S.A.K. acknowledges the Heavy Element Chemistry Program by the Division of Chemical Sciences, Geosciences, and Biosciences, Office of Basic Energy Sciences (BES), U.S. Department of Energy, and Seaborg Institute Postdoctoral Fellowship (S.C.E.S.). LANL is operated by Los Alamos National Security, LLC, for the National Nuclear Security Administration of U.S. DOE (DE-AC52-06NA25396). Use of Stanford Synchrotron Radiation Light source, SLAC National Accelerator Laboratory, supported by DOE, Office of Science, BES (DE-AC02-76SF00515).

REFERENCES

(1) Ravishankara, A. R.; Daniel, J. S.; Portmann, R. W. Nitrous Oxide (N_2O): The Dominant Ozone-Depleting Substance Emitted in the 21st Century. *Science* **2009**, *326*, 123–125.

(2) Reay, D. S.; Davidson, E. A.; Smith, K. A.; Smith, P.; Melillo, J. M.; Dentener, F.; Crutzen, P. J. Global agriculture and nitrous oxide emissions. *Nat. Clim. Change* **2012**, *2*, 410–416.

(3) Thomson, A. J.; Giannopoulos, G.; Pretty, J.; Baggs, E. M.; Richardson, D. J. Biological sources and sinks of nitrous oxide and strategies to mitigate emissions. *Phil. Trans. R. Soc. B* **2012**, *367*, 1157–1168.

(4) Shiro, Y.; Sugimoto, H.; Tosha, T.; Nagano, S.; Hino, T. Structural Basis for Nitrous Oxide Generation by Bacterial Nitric Oxide Reductases. *Phil. Trans. R. Soc. B* **2012**, *367*, 1195–1203.

(5) McQuarters, A. B.; Wirgau, N. E.; Lehnert, N. Model Complexes of Key Intermediates in Fungal Cytochrome P450 Nitric Oxide Reductase (P450nor). *Curr. Opin. Chem. Biol.* **2014**, *19*, 82–89.

(6) Merkle, A. C.; Lehnert, N. Binding and Activation of Nitrite and Nitric Oxide by Copper Nitrite Reductase and Corresponding Model Complexes. *Dalton Trans.* **2012**, *41*, 3355–3368.

(7) (a) Blomberg, M. R. A.; Siegbahn, P. E. M. Mechanism for N_2O Generation in Bacterial Nitric Oxide Reductase: A Quantum Chemical Study. *Biochemistry* **2012**, *51*, 5173-5186. (b) Metz, S. N_2O Formation via Reductive Disproportionation of NO by Mononuclear Copper Complexes: A Mechanistic DFT Study. *Inorg. Chem.* **2017**, *56*, 3820-3833. (c) Suzuki, T.; Tanaka, H.; Shiota, Y.; Sajith, P. K.; Arikawa, Y.; Yoshizawa, K. Proton-Assisted Mechanism of NO Reduction on a Dinuclear Ruthenium Complex. *Inorg. Chem.* **2015**, *54*, 7181–7191.

(8) Arikawa, Y.; Asayama, T.; Moriguchi, Y.; Agari, S.; Onishi, M. Reversible N-N Coupling of NO Ligands on Dinuclear Ruthenium Complexes and Subsequent N_2O Evolution: Relevance to Nitric Oxide Reductase. *J. Am. Chem. Soc.* **2007**, *129*, 14160–14161.

(9) Lionetti, D.; de Ruiter, G.; Agapie, T. A Trans-Hyponitrite Intermediate in the Reductive Coupling and Deoxygenation of Nitric Oxide by a Tricopper-Lewis Acid Complex. *J. Am. Chem. Soc.* **2016**, *138*, 5008-5011.

(10) Wijeratne, G. B.; Hematian, S.; Siegler, M. A.; Karlin, K. D. Copper(I)/NO(g)Reductive Coupling Producing a Trans-Hyponitrite Bridged Dicopper(II) Complex: Redox Reversal Giving Copper(I)/NO(g)Disproportionation. *J. Am. Chem. Soc.* **2017**, *139*, 13276–13279.

(11) Wright, A. M.; Zaman, H. T.; Wu, G.; Hayton, T. W. Mechanistic Insights into the Formation of N_2O by a Nickel Nitrosyl Complex. *Inorg. Chem.* **2014**, *53*, 3108–3116.

(12) (a) Wright, A. M.; Hayton, T. W. Understanding the Role of Hyponitrite in Nitric Oxide Reduction. *Inorg. Chem.* **2015**, *54*, 9330–9341. (b) Arikawa, Y.; Onishi, M. Reductive N-N Coupling of NO Molecules on Transition Metal Complexes Leading to N_2O. *Coord. Chem. Rev.* **2012**, *256*, 468–478.

(13) Fomitchev, D. V.; Furlani, T. R.; Coppens, P. Combined X-Ray Diffraction and Density Functional Study of [Ni(NO)(η^5-Cp*)] in the Ground and Light-Induced Metastable States. *Inorg. Chem.* **1998**, *37*, 1519–1526.

(14) Enemark, J. H.; Feltham, R. D. Principles of Structure, Bonding, and Reactivity for Metal Nitrosyl Complexes. *Coord. Chem. Rev.* **1974**, *13*, 339–406.

(15) Evans, W. J.; Fang, M.; Bates, J. E.; Furche, F.; Ziller, J. W.; Kiesz, M. D.; Zink, J. I. Isolation of a radical dianion of nitrogen oxide $(NO)^{2-}$. *Nat. Chem.* **2010**, *2*, 644–647.

(16) Ohta, K.; Muramoto, K.; Shinzawa-Itoh, K.; Yamashita, E.; Yoshikawa, S.; Tsukihara, T. X-Ray Structure of the NO-Bound CuB in Bovine Cytochrome c Oxidase. *Acta Crystallogr. Sect. F.* **2010**, *66*, 251–253.

(17) Tocheva, E. I.; Rosell, F. I.; Mauk, A. G.; Murphy, M. E. P. Side-on Copper-Nitrosyl Coordination by Nitrite Reductase. *Science* **2004**, *304*, 867–870.

(18) Usov, O. M.; Sun, Y.; Grigoryants, V. M.; Shapleigh, J. P.; Scholes, C. P. EPR-ENDOR of the Cu(I)NO Complex of Nitrite Reductase. *J. Am. Chem. Soc.* **2006**, *128*, 13102–13111.

(19) Fujisawa, K.; Tateda, A.; Miyashita, Y.; Okamoto, K.; Paulat, F.; Praneeth, V. K. K.; Merkle, A.; Lehnert, N. Structural and Spectroscopic Characterization of Mononuclear copper(I) Nitrosyl Complexes: End-on versus Side-on Coordination of NO to copper(I). *J. Am. Chem. Soc.* **2008**, *130*, 1205–1213.

(20) Wasbotten, I. H.; Ghosh. A. Modeling Side-on NO Coordination to Type 2 Copper in Nitrite Reductase: Structures, Energetics, and Bonding. *J. Am. Chem. Soc.* **2005**, *127*, 15384-15385.

(21) Ghosh, S.; Dey, A.; Usov, O. M.; Sun, Y.; Grigoryants, V. M.; Scholes, C. P.; Solomon, E. I. Resolution of the Spectroscopy versus Crystallography Issue for NO Intermediates of Nitrite Reductase from Rhodobacter Sphaeroides. *J. Am. Chem. Soc.* **2007**, *129*, 10310–10311.

(22) Merkle, A. C.; Lehnert, N. The Side-on copper(I) Nitrosyl Geometry in Copper Nitrite Reductase Is due to Steric Interactions with Isoleucine-257. *Inorg. Chem.* **2009**, *48*, 11504–11506.

(23) Puiu, S. C.; Warren, T. H. Three-Coordinate-Diketiminato Nickel Nitrosyl Complexes from Nickel(I)-Lutidine and Nickel(II) - Alkyl Precursors. *Organometallics* **2003**, *22* 3974–3976.

(24) Kundu, S.; Stieber, S. C. E.; Ferrier, M. G.; Kozimor, S. A.; Bertke, J. A.; Warren, T. H. Redox Non-Innocence of Nitrosobenzene at Nickel. *Angew. Chem. Int. Ed.* **2016**, *55*, 10321–10325.

(25) (a) Hayton, T. W.; Legzdins, P.; Sharp, W. B. Coordination and Organometallic Chemistry of Metal-NO Complexes. *Chem. Rev.* **2002**, *102*, 935-991. (b) Böhmer, J.; Haselhorst, G.; Wieghardt, K.; Nuber, B. The First Mononuclear Nitrosyl(oxo)molybdenum Complex: Side-On Bonded and μ_3-bridging NO Ligands in $[\{MoL(NO)(O)(OH)\}_2NaPF_6 \bullet H_2O$. *Angew. Chem. Int. Ed.* **1994**, *20*, 1473–1476.

(26) Neese, F. Orca: an ab initio, DFT and Semiempirical Electronic Structure Package, Version 3.0.3; Max Planck Institute for Chemical Energy Conversion; Mülheim an der Ruhr, Germany.

(27) (a) Tomson, N. C.; Crimmin, M. R.; Petrenko, T.; Rosebrugh, L. E.; Sproules, S.; Boyd, W. C.; Bergman, R. G.; Debeer, S.; Toste, F. D.; Wieghardt, K. A Step Beyond the Feltham-Enenark Notation: Spectroscopic and Correlated *ab Initio* Computational Support for an Antiferromagnetically Coupled M(II)-$(NO)^{\cdot}$ Description of Tp*M(NO)(M = Co, Ni). *J. Am. Chem. Soc.* **2011**, *133*, 18785-18801. (b) Soma, S.; Van Stappen, C.; Kiss, M.; Szilagyi, R. K.; Lehnert, M.; Fujisawa, K. Distorted tetrahedral nickel-nitrosyl complexes: spectroscopic characterization and electronic structure. *J. Biol. Inorg. Chem.* **2016**, *21*, 757-775.

(28) Yao, S.; Bill, E.; Milsmann, C.; Wieghardt, K.; Driess, M. A "side-On" superoxonickel Complex [LNi(O_2)] with a Square-Planar Tetracoordinate Nickel(II) Center and Its Conversion into [LNi(μ-OH)$_2$NiL]. *Angew. Chem. Int. Ed.* **2008**, *47*, 7110–7113.

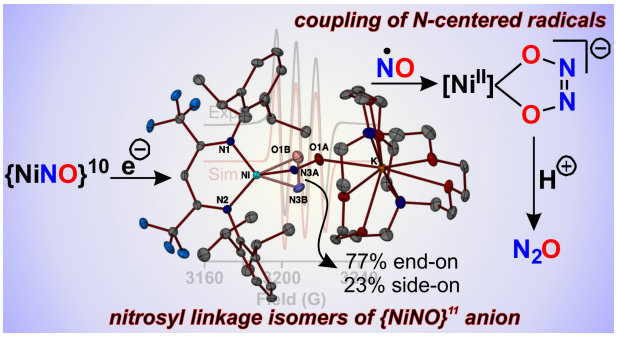
coupling of N-centered radicals
{NiNO}10 e
NO
[NiII]
H
N2O
77% end-on
23% side-on
nitrosyl linkage isomers of {NiNO}11 anion